

# Probabilistic and Possibilistic Analyses of the Strength of a Bonded Joint

W. Jefferson Stroud<sup>1</sup>, T. Krishnamurthy<sup>1</sup> and Steven A. Smith<sup>2</sup>

**Abstract:** The effects of uncertainties on the predicted strength of a single lap shear joint are examined. Probabilistic and possibilistic methods are used to account for uncertainties. A total of ten variables are assumed to be random, with normal distributions. Both Monte Carlo Simulation and the First Order Reliability Method are used to determine the probability of failure. Triangular membership functions with upper and lower bounds located at plus or minus three standard deviations are used to model uncertainty in the possibilistic analysis. The alpha cut (or vertex) method is used to evaluate the possibility of failure. Linear and geometrically nonlinear finite element analyses are used calculate the response of the joint; fracture in the adhesive and material strength failure in the strap are used to evaluate its strength.

Although probabilistic and possibilistic analyses provide significantly more information than do conventional deterministic analyses, they are computationally expensive. A novel scaling approach is developed and used to substantially reduce the computational cost of the probabilistic and possibilistic analyses. The possibilistic approach for treating uncertainties appears to be viable during the conceptual and preliminary design stages when limited data are available and high accuracies are not needed. However, this viability is mixed with several cautions that are discussed herein.

**keyword:** Bonded joint, Probabilistic analysis, Possibilistic analysis, Fracture.

## 1 Introduction

In the final stages of the design of future advanced aerospace vehicles, the design procedures will need to account for uncertainties by calculating the risk or reliability.

These calculations will involve probabilistic analysis. While probabilistic methods may be required in the final stages of design, methods that merely bound a response quantity and provide the most likely value may be adequate for early stages of design. Such methods, referred to herein as possibilistic methods, have the potential for allowing a large number of design options to be evaluated rapidly during the conceptual and preliminary design stages when there may be little data and little need for precision.

When compared with traditional factor-of-safety methods, both probabilistic and possibilistic methods require additional inputs but provide more and higher quality outputs. Variables in these methods can be classified as either certain or uncertain. For probabilistic methods, each uncertain variable is assumed to have a probability density function. In turn, probabilistic methods provide a probability density function for each response quantity. Similarly, possibilistic methods require a membership function for each uncertain variable, and they provide a membership function for each response quantity.

The general objective of this paper is to study the differences between probabilistic and possibilistic methods by exploring their application to a simple and yet commonly encountered structural component. The selected component is a single lap shear joint. The specific objective of the paper is to study how uncertainties affect the predicted strength of a single lap shear joint. The study considers two ways to account for uncertainties (probabilistic and possibilistic), examines the effect of a geometrically nonlinear analysis, shows the effect of two failure modes (fracture in the adhesive and material strength failure in the strap), shows the effect of correlated random variables, and illustrates several computational techniques.

## 2 Description of Lap Joint Problem

The single lap shear joint consists of lap and strap adherends bonded with an adhesive as shown in Fig. 1.

<sup>1</sup> Aerospace Engineer, Analytical and Computational Methods Branch, NASA Langley Research Center, Hampton, VA 23681-2199

<sup>2</sup> Aerospace Engineer, Vehicle Technology Directorate - Army Research Laboratory, Analytical and Computational Methods Branch, NASA Langley Research Center, Hampton, VA 23681-2199

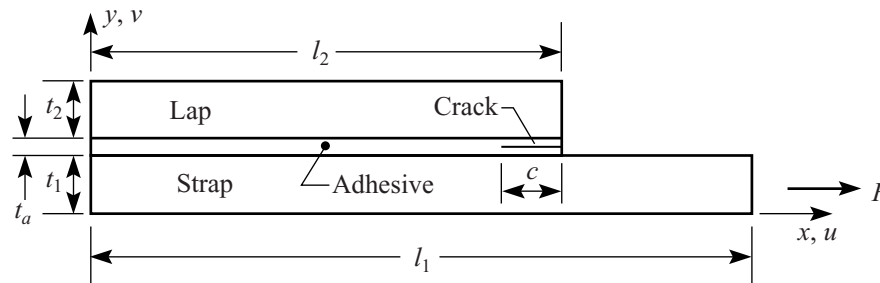


**Figure 1** : Single lap shear joint.

This configuration has been analyzed extensively [Bruscat, Chiu, and Mostvov (1977); Johnson (1987); Lai, Rakestra, and Dillard (1996); Tong and Steven (1999); Mall and Johnson (1985)]. The strap is subjected to a tensile load  $F$  that is reacted at the  $x=0$  plane. The adhesive is assumed to contain a crack of length  $c$  situated centrally within the adhesive. Boundary conditions at the left end of the joint are  $u(0,y) = 0$  and  $v(0,0) = 0$ . These boundary conditions represent symmetry conditions. Boundary conditions at the right end of the strap are  $u(l_1,y) = \text{constant}$  and  $v(l_1,0) = 0$ . These boundary conditions correspond to zero rotation of the face of the strap at the right end and approximate the restraints provided by the grips in a testing machine. Various configurational and material properties that define the single lap shear joint analyzed in this paper are given in Tab. 1. The lap and strap adherends are taken to be 2024 T3 aluminum.

To study the effect of uncertainties, ten of the quantities in Tab. 1 were taken to be independent random variables with normal distributions and with specified means and standard deviations. Two failure modes were considered – fracture in the adhesive due to an existing crack and material strength failure due to yielding in the strap.

### 3 Analysis Approach

This section describes the two approaches that were used to treat uncertainty, the structural analysis method used to analyze the joint, and the two approaches that were used to evaluate failure. Probabilistic and possibilistic approaches were used to treat uncertainty. A commercial finite element code – ABAQUS – was used to analyze the joint. The two failure modes that were used are fracture in the adhesive caused by an existing crack and material strength failure caused by yield in the strap.

#### 3.1 Accounting for Uncertainties

In the probabilistic approach for accounting for uncertainties, ten quantities were assumed to be independent random variables with normal distributions. The random variables and their statistics are given in Tab. 1. With these ten random variables, Monte Carlo simulation (MCS) [Melchers (1999); Elishakoff (1999)] was used to calculate the probability of failure of the joint for various values of the load  $F$ . (A brief description of MCS is presented in Section 4.2.3.) Convergence of the MCS calculations was evaluated by using 100, 1000, and 5000 trials and by comparing these results with results from a FORM analysis. FORM is described in Melchers (1999). The probabilistic analysis code ProFES [Cesare and Sues (1999)] was used for all these calculations.

In the possibilistic approach [Dong and Shah (1987); Nikolaidis, Cudney, Chen, Haftka, and Rosca (1999)], membership functions were assigned to the ten random variables indicated in Tab. 1. An example of a membership function is shown in Fig. 2. The parameter  $\alpha$  indicates the possibility of an uncertain quantity taking on a given value. The objective is to use the membership functions of the input parameters (e.g., dimensions) to determine the corresponding membership functions for the response quantities (e.g., stress, buckling load). Techniques for calculating with membership functions are given in Dong and Shah (1987). The membership functions for the response quantities are then compared with the membership functions of the allowable responses to determine the possibility of failure. In this paper, the membership functions for the ten random variables are taken to be isosceles triangles with the most likely value (MLV in Fig. 2) equal to the mean value given in Tab. 1. The most likely value corresponds to  $\alpha = 1.0$ . The absolute upper and lower bounds (UB and LB in Fig. 2) are equal to the mean value plus/minus three standard

**Table 1** : Values of quantities that define the single lap shear joint

Variable	Symbol	Probabilistic Analysis (normal distributions)		Possibilistic Analysis $\alpha = 0$	
		Mean	Standard Deviation	Lower Bound	Upper Bound
Thickness, strap – in.	$t_1$	0.125	0.005	0.11	0.14
Thickness, lap – in.	$t_2$	0.125	0.005	0.11	0.14
Length, strap – in.	$l_1$	12.0	0	12	12
Length, lap – in.	$l_2$	10.0	0.16	9.52	10.48
Thickness, adhesive – in.	$t_a$	0.0050	0.0005	0.0035	0.0065
Length, crack – in.	$c$	4.00	0.08	3.76	4.24
Modulus, metallic strap – $10^6$ psi	$E_{m1}$	10.5	0.105	10.185	10.815
Modulus, metallic lap - $10^6$ psi	$E_{m2}$	10.5	0.105	10.185	10.815
Poisson’s ratio, metallic lap and strap	$\nu_m$	0.3125	0	0.3125	0.3125
Modulus, adhesive – psi	$E_a$	336,000	16,800	285,600	386,400
Poisson’s ration, adhesive	$\nu_a$	0.40	0	0.4	0.4
Critical value of G (total) – in. lb/in. <sup>2</sup>	$G_c$	5.50	0.66	3.52	7.48
Yield stress 2024 T3 – psi	$\sigma_{yield}$	44,000	880	41,360	46,640
Crack Growth Increment – in.	$\Delta_C$	0.00125	0	0.00125	0.00125

deviations. The absolute upper and lower bounds correspond to  $\alpha = 0.0$  (Tab. 1). A brief discussion of membership functions together with an example that illustrates techniques for calculating with membership functions are presented in Appendix A. Comparisons between probabilistic and possibilistic methods are given in Nikolaidis, Cudney, Chen, Haftka, and Rosca (1999).

To examine the effect of correlated random variables (in contrast with independent random variables), probabilistic calculations were also made under the assumption that  $t_1$  and  $t_2$  are fully correlated and that  $E_{m1}$  and  $E_{m2}$  are fully correlated. In Appendix B, results obtained using these correlated random variables are compared with results obtained using independent random variables.

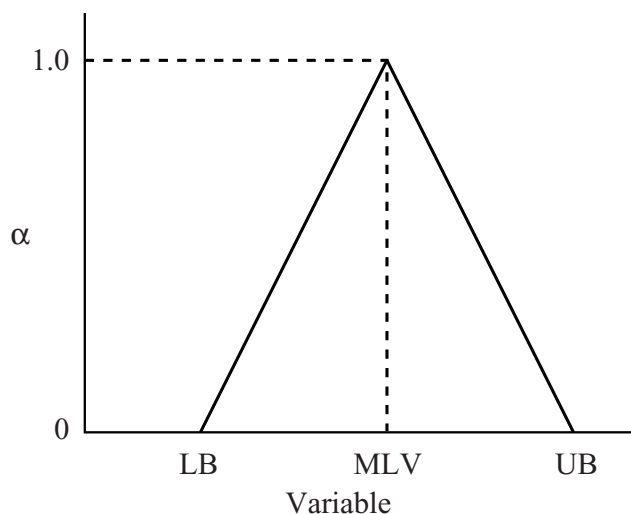
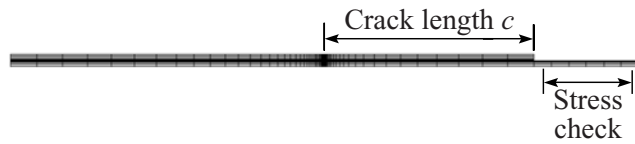


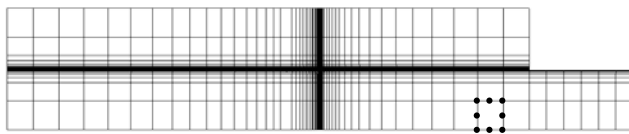
**Figure 2** : Example of membership function.

### 3.2 Finite Element Analysis of Joint

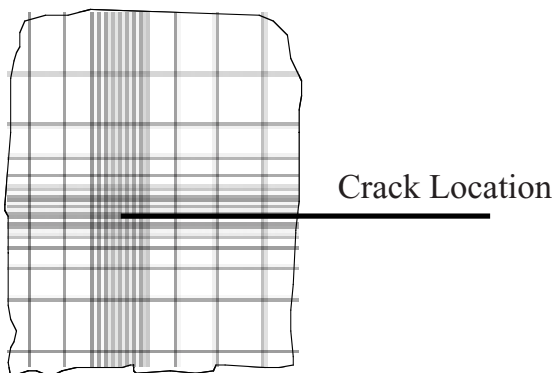
The ABAQUS finite element (FE) structural analysis program [ABAQUS (1998)] was used to analyze the joint. The two-dimensional FE model of the joint (Fig. 3) had 1692 plane strain, 8-node, biquadratic elements (denoted CPE8) with 5331 nodes. These CPE8 elements were used throughout the model, including at and near the crack tip. Near the crack tip, fine mesh modeling is used (Fig. 3(c)), and equal size elements with aspect ratios 1 are maintained on either side of the crack tip to facilitate strain energy release rate calculations. Linear and geometrically nonlinear analyses were carried out. The nonlinear analysis was carried out to study the effects of eccentricity of the loading and the resulting rotation of the joint.



a) FE model.



b) FE model with thickness enlarged to show FE mesh.



c) Detail near the crack tip.

**Figure 3** : FE model of single lap shear joint.

### 3.3 Failure Analysis

#### 3.3.1 Fracture in the Adhesive

The strain energy release rates for self-similar crack growth are used to evaluate fracture in the adhesive due to an existing crack. The evaluation consists of calculating values of the total strain energy release rate  $G_T$  and comparing these values with the experimentally determined value of the critical strain energy release rate  $G_C$  [Reeder, (1992); Reeder (1993)]. Failure is assumed to occur when the total strain energy release rate is equal to or greater than the critical strain energy release rate. Details of the approach used to calculate failure in the adhesive are given in Appendix C.

#### 3.3.2 Material Strength Failure in the Strap

Failure in the strap is assumed to occur when the stress in the strap exceeds the yield stress of the material. The stress was examined in the region denoted “Stress check” in Fig. 3. That region does not include the loaded end, where the boundary conditions may cause local stress perturbations. In the region examined for stress failure, the bending stress is small compared with the extensional stress. (For example, by using a geometrically nonlinear FE analysis it was determined that the bending stress is less than 1% of the extensional stress at  $x = 10$  in., less than 2% at  $x = 11$  in., and less than 6% at  $x = 11.5$  in. The load  $F$  is applied at  $x = 12$  in.) Therefore, after setting to unity the depth of the strap, the stress  $\sigma_x$  is taken to be

$$\sigma_x = \frac{F}{t_1} \quad (1)$$

Note that the calculation of  $\sigma_x$  does not require a FE analysis.

## 4 Results and Discussion

Results of customary deterministic analyses obtained using the mean values of the variables are presented first. Then, results showing the effects of uncertainties are presented.

### 4.1 Deterministic Analyses

The deformed shape of the FE model for a load of 6000 lb is shown in Fig. 4. In the figure, deflections are scaled up by a factor of 10 for visualization purposes. The joint undergoes significant bending.



**Figure 4** : Deformed shape of the lap shear joint obtained using a geometrically nonlinear analysis.

The manner in which the total strain energy release rate  $G_T$  varies with  $F^2$  (the square of the applied load  $F$ ) is shown in Fig. 5. Results for both a linear and a geometrically nonlinear analysis are shown. For perspective, the bounds for the two failure modes – fracture of the adhesive and yield of the strap – are also shown. The value of  $F^2$  corresponding to yield of the strap is given by  $(t_1 \times \sigma_{yield})^2$ . A detailed discussion of the results from the linear and nonlinear analyses is presented in Appendix D.

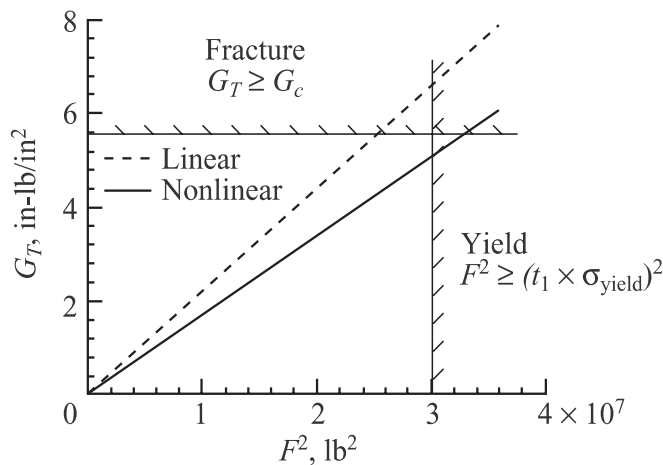


**Figure 5** : Total strain energy release rate  $G_T$  as a function of the square of the applied load. Failure bounds are also shown.

#### 4.1.1 Linear Analysis

As explained in Appendix C, for a linear analysis the forces and displacements that appear in the expressions for the components of the total strain energy release rate  $G_T$  are linear in  $F$ .  $G_T$  is calculated from the sum of the products of these quantities and hence is proportional to  $F^2$ . Thus, the straight line shown in Fig. 5 for the linear case is expected.

#### 4.1.2 Nonlinear Analysis

At first glance, the nonlinear analysis curve in Fig. 5 appears to be a line with a slope different from the slope of the line that defines the linear solution. For that reason, further studies were undertaken to examine the nonlinear solution in detail. These studies are presented in Appendix D. It was concluded that at  $F=0$  the slope of the nonlinear analysis curve is equal to the slope of the line for the linear solution. For values of  $F$  between zero and 2000 lb, the slope of the nonlinear analysis curve becomes smaller as the joint straightens and stiffens. The nonlinear analysis accounts for that straightening and stiffening. For values of  $F$  greater than about 3000 lb,  $G_T$  is nearly linear in  $F^2$  with a slope that is smaller than that calculated from the linear analysis.

#### 4.2 Analysis with Uncertainties

Two distinctly different approaches for treating uncertainties are used – probabilistic and possibilistic. The effects of a geometrically nonlinear analysis and the effects of two failure modes – fracture of the adhesive and yield of the strap – are also considered. First, the convergence for a Monte Carlo simulation (MCS) and a technique for greatly reducing computational effort are presented. Then, results are presented for various combinations of probabilistic and possibilistic analysis, linear and nonlinear analysis, and fracture and yield failure modes. (The headings for each of these sections have the following format: method(s) for handling the uncertainties, failure mode(s), type(s) of analysis.) Finally, probabilistic and possibilistic results are presented for a nonlinear analysis with a combination of both failure modes.

##### 4.2.1 Convergence and Fracture Failure

The primary method that was used to study the effect of uncertainties was MCS. Convergence of the MCS calculations was evaluated using 100, 1000, and 5000 trials and by comparing results from MCS with results from a first order reliability method (FORM). Results for 100, 1000, and 5000 trials are given in Tab. 2. Results are shown for both linear and nonlinear FE analyses. In Tab. 2, the applied load used in the linear analysis was 5000 lb; for the nonlinear analysis the applied load was 6000 lb. (The loads in Tab. 2 are different for the linear and nonlinear analyses because the objective of the analysis was to evaluate convergence in the center portion of each curve.) Based on these results, MCS with

**Table 2** : Convergence study of Monte Carlo Simulation

Analysis Type	Load, F, lb	Probability of Failure by Fracture of Adhesive			
		Monte Carlo Simulation (MCS)			FORM
		n = 100	n = 1000	n = 5000	
Linear	5000	0.515	0.511	0.483	0.483
Nonlinear	6000	0.772	0.763	0.764	0.756

5000 trials was considered to be adequate for the studies presented in this paper. Note that the objective was to obtain convergence in the center portion of each curve. If the emphasis were on an accurate representation of data in the tails, a larger number of trials would have been required.

#### 4.2.2 Probabilistic, Fracture, Linear and Nonlinear

As previously mentioned, for the linear case the total strain energy release rate  $G_T$  varies linearly with respect to  $F^2$ . That is,

$$G_T = kF^2 \quad (2)$$

where  $k$  is a constant. Also, for the nonlinear case,  $G_T$  is nearly linear in  $F^2$  for large values of  $F$ . This fact can be used to significantly reduce the computational resources required to produce curves such as those shown in Fig. 6. In this figure, the probability of failure from fracture of the adhesive is plotted as a function of the applied load  $F$  for both a linear and a nonlinear analysis. Each curve was obtained using scaling of individual trials in a Monte Carlo simulation ( $n = 5000$ ) that was carried out at a single value of the load  $F$ . The details of the scaling technique are presented below in Section 4.2.3. For the linear curve, the single value of the load  $F$  was 5000 lb; for the nonlinear curve, the single value of the load  $F$  was 6000 lb. Results obtained using FORM are included in this figure to confirm the accuracy of the scaling technique. Excellent agreement is obtained between the two sets of results.

#### 4.2.3 Monte Carlo Simulation and Scaling of Strain Energy Release Rate

Monte Carlo simulation involves carrying out a large number of numerical experiments, or trials, with random values of the quantities that are selected to be random

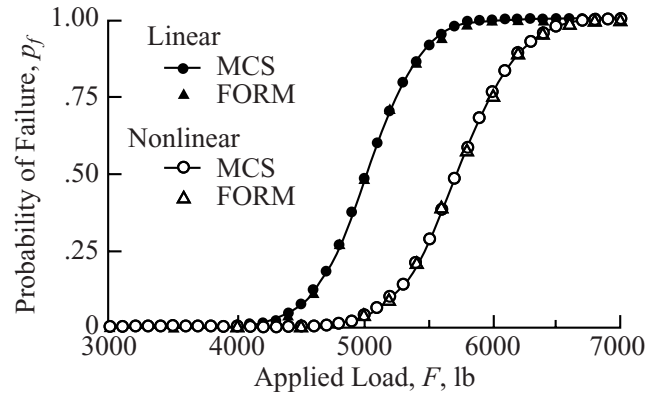


**Figure 6** : Probability of failure by fracture of the adhesive. MCS is carried out using scaling.

variables. In the trials, the randomness of each random variable is guided by the statistics specified for that variable – e.g., type of distribution, mean, and standard deviation.

In the present study, for each Monte Carlo trial a statistically independent configuration of the lap joint is created from the random values of the input variables. A finite element model is developed for that configuration and a finite element analysis is performed to calculate the total strain energy release rate  $G_T$ .

In a given trial, if the calculated value of  $G_T$  exceeds the experimentally determined critical value  $G_C$ , the configuration is considered to have “failed”. For example, if the total number of trials in a simulation is 5000 and if there are 3000 failures, then the probability of failure is 0.6 for this specific load.

Suppose the first Monte Carlo simulation is conducted with  $F = F_0$ . In the general case, in order to obtain the probability of failure for a different load  $F_1$ , the Monte Carlo simulation would have to be repeated for the new load value. However, by utilizing the fact that  $G_T$  is linear with respect to  $F^2$ , it is possible to substantially reduce the computational effort. For each trial, the value of

$G_T$ , for all loads  $F = F_1$ , can be calculated by scaling the value of  $G_T$  calculated for  $F = F_0$ . The scaling is carried out in the following way:

$$G_T|_{F=F_1} = \left(\frac{F_1}{F_0}\right)^2 G_T|_{F=F_0} \quad (3)$$

The value of  $G_T$  obtained through scaling for each trial is compared with the corresponding value of  $G_C$ . The number of failures is counted to calculate the probability of failure for the current load,  $F = F_1$ . Hence, it is sufficient to perform the Monte Carlo simulation only once for an arbitrary load. The probability of failure for any other load can be calculated by scaling  $G_T$  for each specific trial.

In the present study, scaling of  $G_T$  is used to calculate the probability of failure for both linear and nonlinear FE analyses.

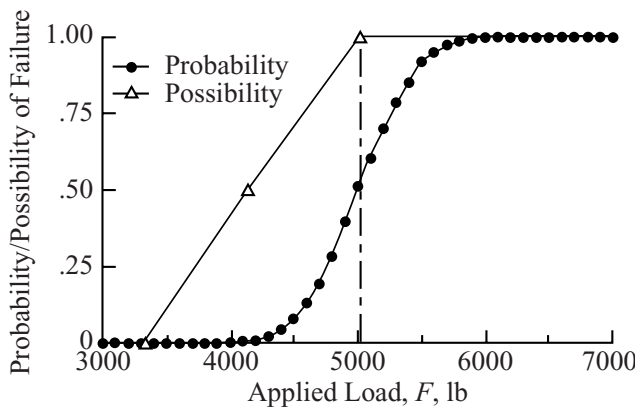


**Figure 7** : Possibility and probability of failure by fracture of the adhesive for a linear analysis.

4.2.4 Possibilistic and Probabilistic, Fracture, Linear

Fig. 7 shows the possibility and probability of failure of the joint by fracture of the adhesive for a linear FE analysis. Here and elsewhere in this paper, for a given load the possibility of failure is always greater than the probability of failure. Also note that, for this case, the possibility of failure is 1.00 when the probability of failure ( $p_f$ ) is 0.50. The probability of failure  $p_f$  reaches 0.50 when the load  $F$  is 5015 lb. In the next section, this value is compared with the value obtained using a nonlinear analysis.

4.2.5 Possibilistic and Probabilistic, Fracture, Linear and Nonlinear

Fig. 8 shows the possibility and probability of failure of the joint caused by fracture of the adhesive using both linear and nonlinear FE analyses. Compared with the curves for the linear analysis, the curves for the nonlinear analysis are shifted to the right. For a nonlinear analysis with  $p_f = 0.50$ , the load  $F$  is 5709 lb. Recall from the previous section that the linear analysis predicts a value of 5015 lb. According to these results and the results presented in Fig. 5, a nonlinear analysis predicts that the joint can carry more load than a linear analysis – i.e., a linear analysis is more conservative. Further studies carried out in this paper are based on a nonlinear FE analysis.

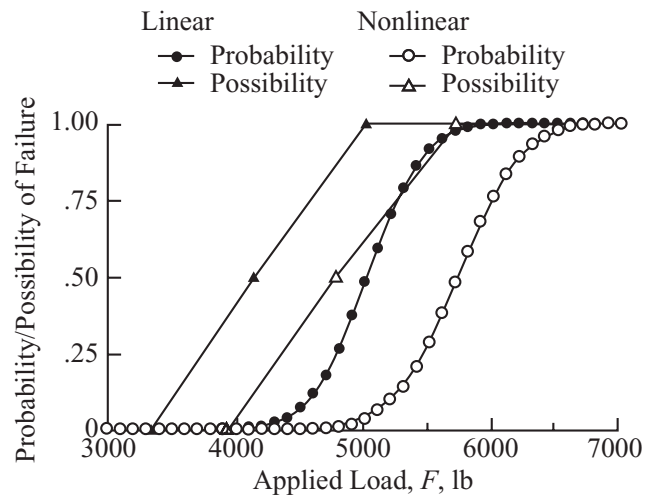
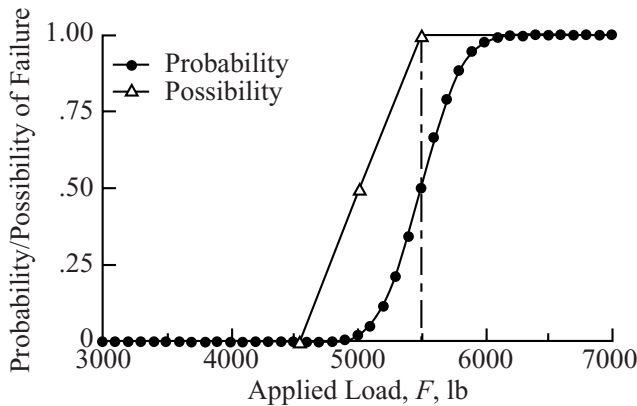


**Figure 8** : Possibility and probability of failure caused by fracture of the adhesive for both a linear and a nonlinear analysis.

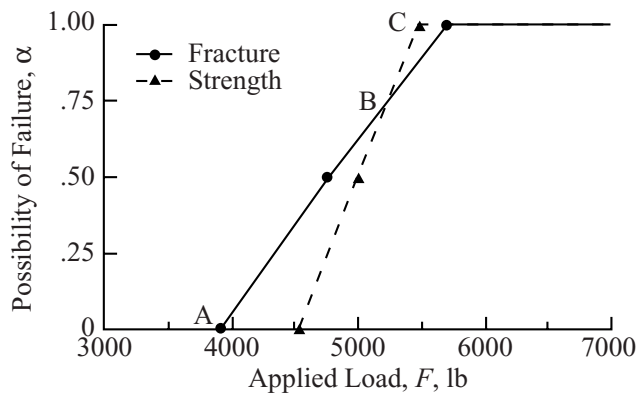
4.2.6 Possibilistic and Probabilistic, Material Strength

Fig. 9 shows the possibility and probability of failure of the joint by material strength failure of the strap (stress  $\sigma_x$  greater than yield stress  $\sigma_{yield}$ ). These results are based on equation (1) and do not require a FE analysis. For  $p_f = 0.50$ , the value of the load  $F$  is 5500 lb, which is less than the value of 5709 lb for the nonlinear fracture failure mode given in the previous section. The results shown in Figs. 7 – 9 are confirmed in Fig. 5 which shows that, for a nonlinear analysis using mean values of the uncertain parameters, material strength failure occurs at a lower load than fracture failure; for a linear analysis

using mean values of the uncertain parameters, fracture occurs at a lower load than material strength failure.



**Figure 9** : Possibility and probability of material strength failure of the strap.



**Figure 10** : Possibility of failure by material strength and by fracture of the adhesive, plotted individually.

4.2.7 Possibilistic, Fracture and Material Strength, Nonlinear

Fig. 10 shows the possibility of failure of the joint by fracture of the adhesive (solid line) and by material strength failure of the strap (dashed line). The possibilistic failure envelope that considers both failure modes is the maximum of the possibilities of the two failure modes. (In the general case, the possibility of failure is the maximum of the possibilities of all the failure modes.) In this case, the possibilistic curve that considers both failure modes starts at  $\alpha = 0$  (point A) with the fracture possibilistic curve – the solid line. It follows

that line up until the line crosses the strength possibilistic curve – the dashed line – at about  $\alpha = 0.75$  (point B). There, the possibilistic curve that considers both failure modes shifts to the strength possibilistic curve (line BC) because, for that value of the applied load  $F$ , failure by material strength of the strap begins to have a higher possibility than failure by fracture of the adhesive. In a possibilistic approach for handling uncertainty, if a failure mode does not have the maximum possibility for some value of the applied load, it has no effect on the possibility of failure. In contrast, in a probabilistic approach for handling uncertainty, secondary failure modes do affect the probability of failure, as discussed below.

4.2.8 Probabilistic, Fracture and Material Strength, Nonlinear

Fig. 11 shows the probability of failure of the joint by fracture of the adhesive and by material strength failure of the strap. Three curves are shown. The first curve (filled circular symbols) is for failure of the joint by fracture of the adhesive. The second curve (filled triangular symbols) is for material strength. The third curve (open square symbols) is for either of the two failure modes or both modes – i.e., the third curve is the union of the two failure events. In the probabilistic approach for calculating the probability of failure caused by a combination of the two failure modes, both failure modes have an effect on the probability of failure, not just the more critical mode. This phenomenon can be seen in Fig. 11, where the third curve is to the left of either of the two curves for the individual failure modes – i.e., the third curve indicates a higher probability of failure than either of the other two curves.

The effect of two failure modes on the probability of failure is indicated mathematically as

$$p_f(X \cup Y) = p_f(X) + p_f(Y) - p_f(X \cap Y) \tag{4}$$

where  $X$  indicates failure by the first failure mode and  $Y$  indicates failure by the second failure mode. Finally, if there were additional failure modes, the curve that accounts for all modes would shift further to the left. That is, for a given load, that curve would indicate a higher probability of failure than the curves for any of the individual failure modes.



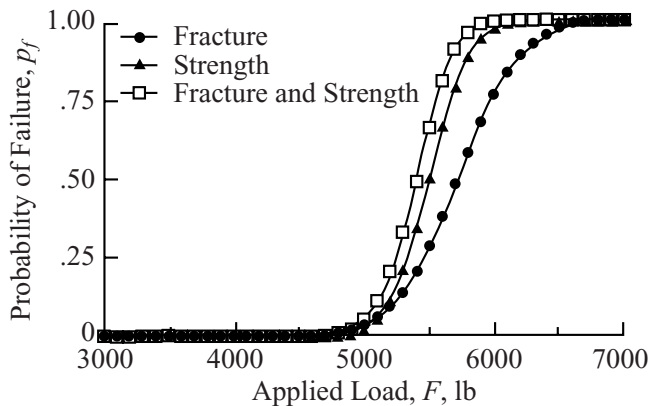


**Figure 11** : Probability of failure by material strength and fracture, plotted individually and in combination.

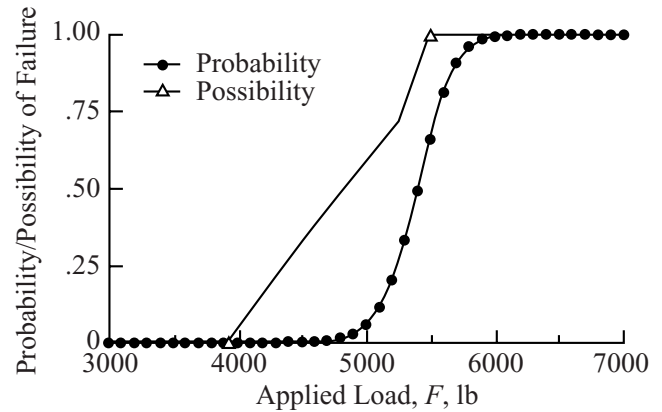


**Figure 12** : Possibility and probability of failure by combined material strength and fracture. (Nonlinear analysis).

4.2.9 Probabilistic and Possibilistic, Fracture and Material Strength, Nonlinear

The results of the study are summarized in Fig. 12, which shows the possibility and probability of failure of the joint by fracture of the adhesive and by material strength failure of the strap. Both curves are for a geometrically nonlinear analysis. The possibilistic curve shows the change in slope where the maximum possibility shifts from fracture of the adhesive to material strength failure of the strap. The possibility of failure becomes 1.0 at a load  $F$  of 5500 lb. The probability of failure at that load is 0.66. (In previous calculations presented in this paper, the possibility of failure becomes 1.0 when the probability of failure is 0.50. The combination of two failure modes causes that pattern to change.) The probability of failure is 0.50 at a load  $F$  of 5405 lb. For all values of the load  $F$ , the possibility of failure is greater than the probability of failure.

5 Effect of Interchanging Distributions of Random Variables

To insure that the differences between the probabilistic and possibilistic results are due primarily to the differences in the methods, rather than to the differences in the distributions of the random variables, additional studies were carried out. In these studies, the distributions of the random variables were interchanged. That is, the random variables for the probabilistic analyses were given a triangular distribution, and the random variables for the possibilistic analyses were given a normal distribution.

Some of the calculations were then rerun. The modified distributions and results are given below.

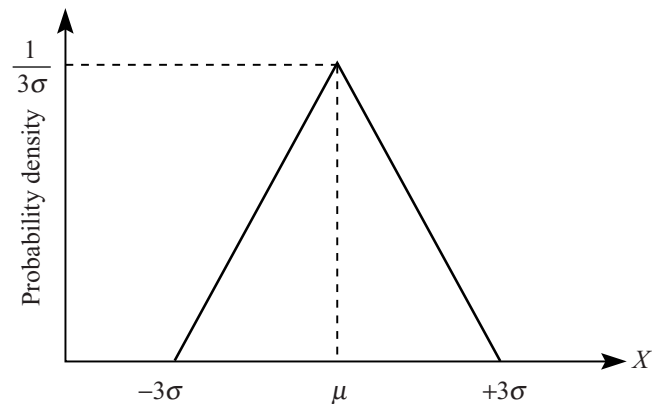


**Figure 13** : Triangular distribution for probabilistic analysis.

The distributions for the probabilistic and possibilistic analyses are shown in Figs. 13 and 14, respectively. The triangular distribution (Fig. 13) for the probabilistic random variables is the same as the distribution shown in Fig. 2, except that the vertical dimension is scaled so that the area under the triangle is equal to unity. The normal distribution (Fig. 14) for the possibilistic random variables is the same as the usual normal distribution except that the vertical dimension is scaled so that the highest point is equal to unity. In Figs. 13 and 14, the horizontal axis gives the value of the random variable, denoted  $x$ . The mean value of the random variable is denoted  $\mu$ , and the standard deviation is denoted  $\sigma$ .

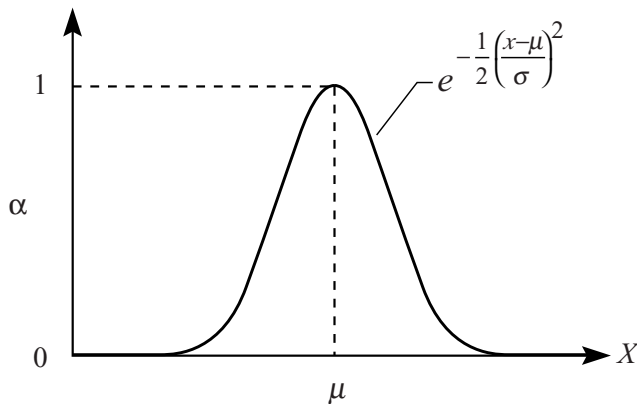


**Figure 14 :** Scaled normal distribution for possibilistic analysis.

Results for the new distributions are presented in Figs. 15 and 16. Results are presented in Fig. 15 for the probability and possibility of failure caused by fracture of the adhesive for a nonlinear analysis. For comparison, results for the nonlinear case shown in Fig. 8 are plotted as dashed curves. Results are presented in Fig. 16 for the probability and possibility of failure caused by combined material strength and fracture for a nonlinear analysis. For comparison, the results from Fig. 12 are included in the figure.

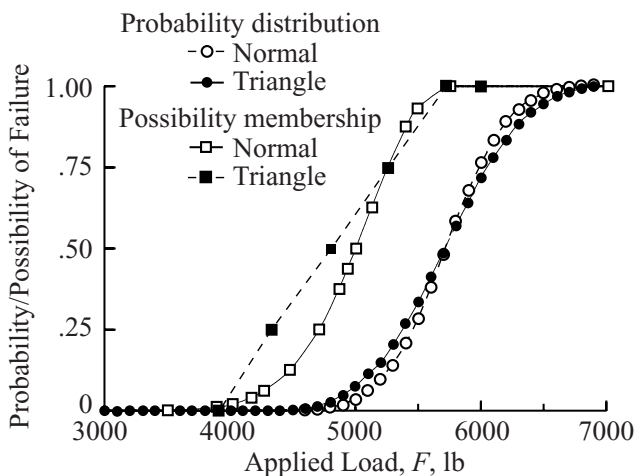


**Figure 15 :** Probability and possibility of failure by fracture of the adhesive. Nonlinear analyses.

The results shown in Figs 15 and 16 indicate that for the general position of either the probabilistic or possibilistic failure curves, the exact definition of the distributions of random variables is not critical. For example, when

comparing the loads associated with a given probability of failure in the load range for which the probability of failure varies from 0.1 to 0.9, the difference between the probabilistic results obtained using the triangular and normal distributions is less than 3%. Differences are larger for the possibilistic results. Also, defining the tails of the failure curves requires more precision.

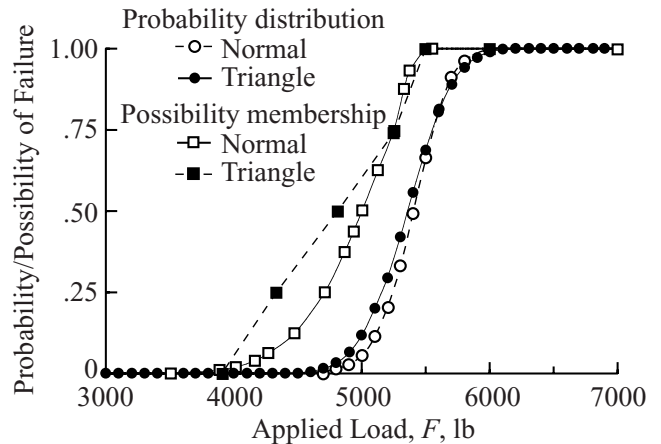


**Figure 16 :** Probability and possibility of failure by combined material strength and fracture of the adhesive. Nonlinear analyses.

Based on these results, it can be concluded that the differences between the probabilistic and possibilistic results presented in this paper are due primarily to the differences in the methods, and not to the differences in the distributions of the random variables. Furthermore, it can be concluded that for the general position of either the probabilistic or possibilistic failure curves, the exact definition of the distributions of random variables is not critical. This conclusion is important for conceptual and preliminary design stages when there may be little data and little need for precision. It means that approximate distributions can be useful in early design.

## 6 Discussion of Probabilistic and Possibilistic Methods

Based on the discussions in the previous three sections, the following contrasts can be drawn between probabilistic and possibilistic methods. Suppose a structure has many failure modes, any of which can cause the structure to fail – i.e., the structure is a series system. (The single lap shear joint with two failure modes is an example of a

series system.) In a probabilistic analysis the probability of failure increases with each failure mode considered. In contrast, in a possibilistic analysis the possibility of failure increases only if a failure mode is introduced that has a larger possibility of failure than any other failure mode. For example, suppose that the structure is a chain of identical links. The probability of failure increases with increasing chain length. In contrast, the possibility of failure remains the same regardless of chain length. As a result, for multiple failure modes a possibilistic analysis may become unconservative.

Using the same reasoning, a possibilistic approach could exhibit unexpected behavior for a structure with redundancies – i.e., a parallel system. The probability of failure of the structural system is reduced as the redundancy is increased. In contrast, the possibility of failure of the structural system is equal to the possibility of failure of the component having the largest possibility of failure – regardless of the number of redundancies. As a result, for redundant systems a possibilistic approach is conservative. An excellent in-depth discussion of probabilistic versus possibilistic methods is presented in Nikolaidis, Cudney, Chen, Haftka, and Rosca (1999).

Possibilistic approaches for treating uncertainties may be viable for early design. But it is not clear that possibilistic approaches are superior to probabilistic approaches for early design. For example, whereas the number of function evaluations for a possibilistic analysis may be small compared with a Monte Carlo simulation, the number of function evaluations may be comparable to that required by some probabilistic methods such as FORM. These probabilistic methods can provide more information than possibilistic methods. Furthermore, even though the possibility of failure was always greater than the probability of failure for the bonded joint example with two failure modes, the assumption that possibilistic design is conservative is not a valid assumption when there are many failure modes. In many cases, the choice of methods depends upon the availability of data. Finally, the choice of methods depends upon the designer.

## 7 Concluding Remarks

This paper has explored the effects of configuration and material uncertainties on the predicted strength of a single lap shear joint. Finite element analyses were used to study the joint. The study contrasts two ways to account for uncertainties (probabilistic and possibilistic), shows

the effect of two failure modes (fracture in the adhesive and material strength failure in the strap), examines the effect of a geometrically nonlinear analysis, shows the effect of correlated random variables, and illustrates several computational techniques.

Probabilistic methods have a strong mathematical background, and the results are well understood. However, probabilistic methods require substantial data and can be computationally expensive. To overcome these shortcomings, possibilistic methods have been proposed for preliminary and conceptual design because these methods may have the potential for allowing a large number of design options to be evaluated rapidly during the early design stages when there may be little data and little need for precision. Based on studies presented here and elsewhere, it appears that possibilistic methods are viable for early design, but there are several qualifications. For example, possibilistic results may not be easy to interpret, possibilistic methods can be computationally expensive, and there can be questions about conservatism when there are many failure modes. As a result of these qualifications, it is not clear that possibilistic approaches are superior to probabilistic approaches for early design. The primary reason for using possibilistic methods appears to be that these methods require less data than probabilistic methods.

For the calculations presented herein, differences in results produced by probabilistic and possibilistic methods are due primarily to differences in the methods rather than to differences in the distributions (normal vs. triangular) used by the two methods to describe the uncertain quantities. Furthermore, it can be concluded that for the general position of either the probabilistic or possibilistic failure curves, the exact definition of the distributions of random variables is not critical. This means that approximate distributions can be useful in early design.

Having two failure modes provided an opportunity to contrast the probabilistic and possibilistic approaches for treating multiple failure modes. In a possibilistic approach for handling uncertainty, if a failure mode does not have the maximum possibility for some value of the applied load, it has no effect on the possibility of failure. In contrast, in a probabilistic approach for handling uncertainty, secondary failure modes do affect the probability of failure.

Geometrically nonlinear analyses are essential for accurately predicting the probability and possibility of failure of the single lap shear joint. The failure load predicted by the geometrically nonlinear analysis is larger than the failure load predicted by the linear analysis.

A novel computational technique helped make the calculations tractable. For a linear analysis, the strain energy release rates are proportional to the square of the applied load. For a geometrically nonlinear analysis, the strain energy release rates are almost proportional to the square of the applied load for large values of the applied load. These characteristics make it possible to employ scaling to substantially reduce computational effort.

#### Acknowledgements:

During this research, valuable discussions were held with several of the authors' colleagues. These include Drs. Ivatury Raju, Raphael Haftka, Justin Wu, Efstratios Nikolaidis, Isaac Elishakoff, Kevin O'Brien, and Ronald Krueger.

#### References

- ABAQUS** Users Manual, Version 5.8, (1998): Hibbitt, Karlsson, and Sorensen, Inc., 1080 Main Street, Pawtucket, RI 02860-4847.
- Brussat, T. R.; Chiu, S. T.; Mostvov, S.** (1997): "Fracture Mechanics for Structural Adhesive Bonds – Final Report," AFML-TR-77-163, Air Force Materials Laboratory, Wright Patterson Air Force Base, Dayton, OH.
- Cesare, Mark, A.; Sues, Robert, H.** (1999): "PROFES Probabilistic Finite Element System-Bringing Probabilistic Mechanics to the Desktop", *Proceedings of 40th AIAA/ASME/ASCE/AHS/ASC Structures, Structural Dynamics, and Materials Conference*, April 12-15, 1999, St. Louis, MO, Paper No. AIAA-99-1607, 1999.
- Dong, W.; Shah, H.C.** (1987): "Vertex Method for Computing Functions of Fuzzy Variables," *Fuzzy Sets and Systems*, 24, pp. 65-78.
- Elishakoff, Isaac** (1999): "Probabilistic Theory of Structures," Second Edition, Dover Publications, Inc., Mineola, NY.
- Johnson, W. S.** (1987): "Stress Analysis of the Cracked-Lap-shear Specimen: An ASTM Round-Robin," *J. of Testing and Evaluation*, Vol. 15, pp. 303-324.
- Krueger, R.; Minguet, P. J.; O'Brien, T. K.** (2000): "A Method for Calculating Strain Energy Release Rates in Preliminary Design of Composite Skin/Stringer Debonding Under Multiaxial Loading," *Composite Structures: Theory and Practice*, ASTM STP 1383, P. Grant and C. Q. Rousseau, Eds., American Society for Testing and Materials, West Conshohocken, PA, pp. 105-128.
- Lai, Y. H.; Rakestra, M. D.; Dillard, D. A.** (1996): "The Cracked Lap Shear Specimen Revisited - A Closed Form Solution," *Int. J. of Solids and Structures*, Vol. 33, No. 12, pp. 1725-1743.
- Mall, S.; Johnson, W. S.** (1985): "Characterization of Mode I and Mixed Mode Failure of Adhesive Bonds Between Composite Adherends," NASA Technical Memorandum 86355.
- Melchers, R. E.** (1999): "Structural Reliability, Analysis and Prediction," Chichester; New York: John Wiley.
- Nikolaidis, Efstratios; Cudney, Harley; Chen, Sophie; Haftka, Raphael T.; Rosca, Raluca** (1999): "Comparison of Probabilistic and Possibility Theory-Based Methods for Design Against Catastrophic Failure Under Uncertainty," *Proceedings of the 1999 ASME Design Engineering Technical Conferences, 11th International Conference on Design Theory and Methodology*, Sept. 12-15, 1999, Las Vegas, Nevada. Available as DETC99/DTM-8758.
- Raju, I. S.** (1987): "Calculation of Strain-Energy Release Rates with Higher Order and Singular Finite Elements," *Engineering Fracture Mechanics*, Vol. 28, No. 3, pp. 251-274.
- Ramamurthy, T. S.; Krishnamurthy, T.; Narayana, K. B.; Vijayakumar, K.; Dattaguru, B.** (1986): "Modified Crack Closure Integral Methods With Quarter Point Elements," *Mech. Res. Commun.*, Vol. 13, pp. 179-286.
- Reeder, J. R.** (1992): "An Evaluation of Mixed-Mode Delamination Failure Criteria," NASA-TM-104210.
- Reeder, J. R.** (1993): "Bilinear Fracture Criterion for Mixed-Mode Delamination," *Composite Materials: Testing and Design-11<sup>th</sup> Volume*, ASTM STP 1206, American Society for Testing and Materials, West Conshohocken, PA, 1993, p. 303-322. Also available as NASA-TM-111543.
- Rybicki, E. F.; Kanninen, M. F.** (1977): "A Finite Element Calculation of Stress-Intensity Factors by a Modified Crack Closure Integral," *Engineering Fracture Mechanics*, Vol. 9, pp. 931-938.

**Smith, S.A.; Raju, I.S.** (1998): "Evaluation of Stress-Intensity Factors Using General Finite-Element Models," *Fatigue and Fracture Mechanics: Twenty-Ninth Volume*, ASTM STP 1332, T.L. Pantoin, and S.D. Sheppards, Eds., American Society for Testing and Materials, West Conshohocken, PA, pp. 176-199.

**Tong, L.; Steven, G. P.** (1999): "*Analysis and Design of Structural Bonded Joints*," Kluwer Academic Publishers, Boston/Dordrecht/London.

**Appendix A: Calculating with Membership Functions**

Let  $\alpha$  be a parameter that indicates the possibility of an uncertain quantity taking on a given value. The parameter  $\alpha$  takes on values between zero and one. A value of zero indicates no possibility, while a value of one indicates maximum possibility. A membership function describes the relationship between  $\alpha$  and the possible values of the uncertain quantities. An example of a membership function is shown in Fig. 2. In a possibilistic analysis, each of the uncertain quantities that contribute to the response is defined in terms of a membership function. The objective of the possibilistic analysis is to determine the corresponding membership function of the response quantities. The membership functions of the response quantities can then be compared with the membership functions for the allowable responses to determine the possibility of failure.

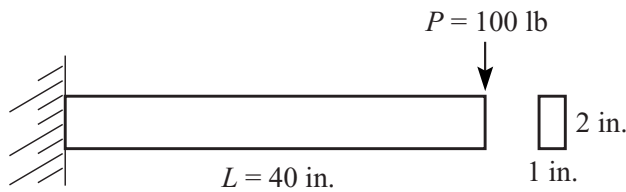


**Figure A1.** Cantilever beam example.

A simple example is used to illustrate how to perform calculations using membership functions. Consider the cantilever beam shown in Fig. A1. The tip deflection  $\delta$  is given by

$$\delta = \frac{PL^3}{3EI} \tag{A1}$$

where  $P$  is the load at the tip,  $L$  is the length,  $E$  is Young's modulus, and  $I$  is the moment of inertia. Assume that  $L$  and  $I$  are uncertain quantities with membership functions similar to that shown in Fig. A2. The vertical scale is the possibility, denoted  $\alpha$ , which varies from zero to one. The values of  $E$  and  $P$  are taken to be  $10^7$  psi and 100 lb, respectively.

The membership functions for  $L$  and  $I$  are isosceles triangles with upper and lower bounds (UB, LB) shown in Tab. A1. The bounds are for  $\alpha = 0.0, 0.5,$  and  $1.0$ . The objective is to obtain an estimate of the uncertainty in  $\delta$  by calculating its membership function.

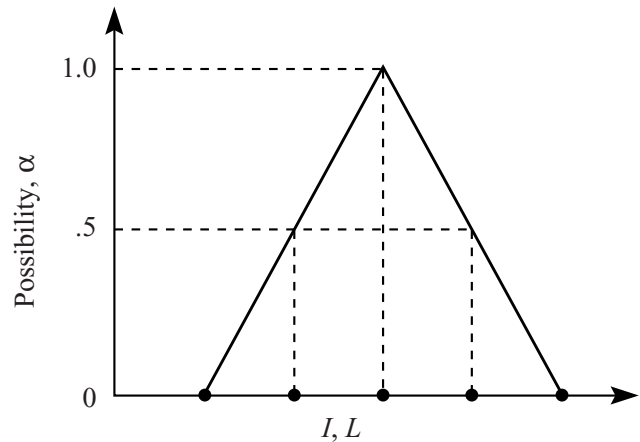


**Figure A2.** Example membership function for moment of inertia  $I$  and length  $L$  of cantilever beam example. (Filled circles bounds on  $I$  and  $L$  corresponding to  $\alpha = 0.0, 0.5,$  and  $1.0$ ).

To obtain the upper and lower bounds for  $\delta$  at  $\alpha = 0.0$ , calculate  $\delta$  for various combinations of  $L$  and  $I$  within their  $\alpha = 0.0$  bounds and select the largest and smallest values. That is, calculate  $\delta$  for several combinations of  $L$  and  $I$  in the ranges  $39.8 \leq L \leq 40.2$  and  $0.64583 \leq I \leq 0.68750$ . To obtain the upper and lower bounds for  $\delta$  at  $\alpha = 0.5$ , calculate  $\delta$  for various combinations of  $L$  and  $I$  within their  $\alpha = 0.5$  bounds and select the largest and smallest values. That is, calculate  $\delta$  for several combinations of  $L$  and  $I$  in the ranges  $39.9 \leq L \leq 40.1$  and  $0.65625 \leq I \leq 0.67708$ . The same approach is used for other values of  $\alpha$ . To obtain the most likely value of  $\delta$ , which is the value corresponding to  $\alpha = 1.0$ , use the most likely values of  $L$  and  $I$ , 40.0 and 0.66667, respectively.

**Table A1.** Assumed bounds on independent variables  $I$  and  $L$  and corresponding calculated bounds for tip deflection of cantilever beam example

$\alpha$	$I$ in. <sup>4</sup>		$L$ in.		$\delta$ in.	
	LB	UB	LB	UB	LB	UB
0.0	0.64583	0.68750	39.800	40.200	0.30567	0.33530
0.5	0.65625	0.67708	39.900	40.100	0.31272	0.32752
1.0	0.66667	0.66667	40.000	40.000	0.32000	0.32000

For this simple example it is easy to select the values of  $L$  and  $I$  that give the upper and lower bounds on  $\delta$ . The upper bound on  $\delta$  is given by a combination of the upper bound on  $L$  and the lower bound on  $I$ . The lower bound on  $\delta$  is given by a combination of the lower bound on  $L$  and the upper bound on  $I$ . In general, to calculate the upper and lower bounds on a response quantity at a given value of  $\alpha$  it is necessary to use *several* combinations of values of the independent variables at that same value of  $\alpha$ . These values include both the bounds and values between the bounds. It cannot be assumed that bounds on the response quantities can be identified by considering only the bounds on the independent variables.

### Appendix B: Effect of Correlated Variables

In the body of this paper, the random variables are assumed to be independent – that is, the value of each random variable is assumed to be independent of the values of the other random variables. This appendix describes probabilistic calculations that were made under the assumption that some of the random variables are correlated – that is, the values of these random variables depend upon the values of other random variables. Results were obtained using a nonlinear finite element analysis described in the body of the paper.

The probabilistic calculations described in this appendix were made under the assumption that the thicknesses of the lap and strap ( $t_1$  and  $t_2$ ) are fully correlated and that the Young's moduli of the lap and strap ( $E_{m1}$  and  $E_{m2}$ ) are fully correlated. This means that  $t_1 = t_2$  and  $E_{m1} = E_{m2}$ .

Because material strength failure in the strap depends only upon the force  $F$ , the strap thickness  $t_1$ , and the yield stress of the strap  $\sigma_{yield}$ , the assumed correlation has no effect on the probability of failure by material strength failure – i.e., Fig. 9 is not affected. The assumption that  $t_1$  and  $t_2$  are fully correlated and that  $E_{m1}$  and  $E_{m2}$  are fully

correlated does have a small effect on the probability of failure by fracture of the adhesive. That effect is shown in Fig. B1 and in Tab. B1.

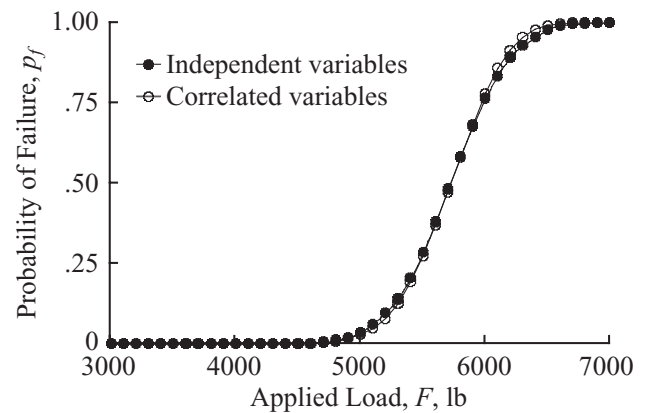


**Figure B1:** Probability of failure by fracture of the adhesive, for independent random variables and correlated random variables.

Fig. B1 shows the probability of failure by fracture of the adhesive for the cases of independent random variables and correlated random variables. As can be seen in Tab. B1, the mean value of the failure load is about the same for the correlated variable case as it is for the independent variable case. However, the standard deviation is smaller for the correlated variable case than it is for the independent variable case. (There is less uncertainty in the correlated case.)

Fig. B2 shows the probability of failure considering both material strength and fracture and for both independent and correlated random variables. For a given load, the probability of failure is slightly higher if the variables are independent.

**Table B1:** Effect of correlated random variables on the statistics of failure for cases of failure by fracture of the adhesive and by combined fracture of the adhesive and material strength of the strap.

Failure mode	Independent random variables		Correlated random variables	
	Mean	Standard deviation	Mean	Standard deviation
Fracture	5766.7	393.6	5765.2	361.3
Combined fracture and strength	5443.0	242.9	5478.3	252.7

**Table B2:** Illustration of how Monte Carlo simulation is used to calculate individual and system probability of failure for a series system. Failure by Fracture or Strength causes system failure – here denoted Combined. F indicates failure for a trial; 0 indicates survival.

Trial No.	Case A			Case B		
	Fracture	Strength	Combined	Fracture	Strength	Combined
1	0	F	F	F	F	F
2	F	0	F	0	0	0
3	F	F	F	F	F	F
4	0	0	0	0	0	0
5	0	F	F	F	F	F
6	F	F	F	F	F	F
7	F	0	F	F	0	F
Total Failures	4	4	6	5	4	5
<i>P</i> (failure)	0.57	0.57	0.86	0.71	0.57	0.71

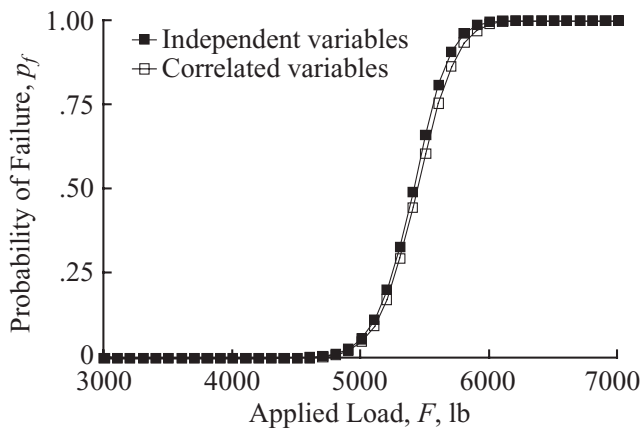


**Figure B2:** Probability of failure considering both materials strength and fracture of the adhesive, for independent random variables and correlated random variables.

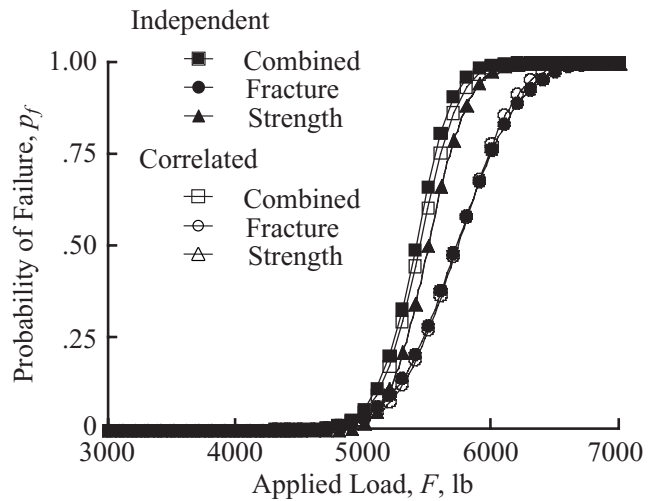


**Figure B3:** Probability of failure considering both material strength and fracture of the adhesive, plotted individually and in combination, for independent random variables and correlated random variables.

Fig. B3 combines the curves shown in Figs. B1 and B2 with the curve giving the probability of material strength failure.

For loads greater than about 5800 lb, correlation slightly increases the probability of failure by fracture. In contrast, if both fracture and material strength failures are considered, correlation slightly decreases the probability of failure. One explanation for this counterintuitive result involves the procedure used in a Monte Carlo simulation to calculate individual and system probabilities of failure for a series system. (See sections 4.2.3 and 6.) In that load range, even though correlation resulted in an increase in trials having fracture failure, correlation also produced an even greater increase in the number of trials in which both fracture and strength failures occurred. Since strength failure was not affected by correlation, the number of trials having system failure decreased, resulting in a lower probability of system failure. This situation is illustrated in Tab. B2. Compared with Case A, Case B has a higher probability of fracture failure, but a lower probability of failure considering both fracture and strength.

The curves in Fig. B3 emphasize the fact that material strength failure is the dominant failure mode and that correlation of the selected random variables has only a small effect on the probability of failure.

### Appendix C: Approach Used to Calculate Fracture in the Adhesive

It was stated in section 3.3.1 that the strain energy release rates for self-similar crack growth are used to evaluate fracture in the adhesive due to an existing crack. This appendix provides details of that evaluation.

The evaluation consists of calculating values of the total strain energy release rate  $G_T$  and comparing these values with the experimentally determined value of the critical strain energy release rate  $G_C$  [Reeder, (1992); Reeder (1993)]. Failure is assumed to occur when the total strain energy release rate is equal to or greater than the critical strain energy release rate, i.e.,

$$G_T \geq G_C \tag{C1}$$

For this joint configuration, the total strain energy release rate  $G_T$  is given by

$$G_T = G_I + G_{II} \tag{C2}$$

where  $G_I$  and  $G_{II}$  are the strain energy release rates for mode-I and mode-II failures, respectively. The critical



strain energy release rate in equation (C1) for mixed-mode fracture is dependant on the mode-mixity [Reeder, (1992); Reeder (1993)]. The critical strain energy release rate used in this paper is for FM-300 adhesive tested in mixed-mode conditions with a mode-mixity,  $G_I/G_{II} = 0.3$  [Mall and Johnson (1985)].

The “virtual crack closure technique” (VCCT) is used to evaluate  $G_I$  and  $G_{II}$  using the crack tip forces and the opening and sliding displacements of the crack faces [Rybicki and Kanninen (1977); Raju (1987); Ramamurthy, Krishnamurthy, Narayana, Vijayakumar, and Dattaguru (1986); Smith and Raju (1998); Krueger, Minguet, and O’Brien (2000)]. Due to large rotations of the model in the vicinity of the crack tip, a nonlinear formulation of the VCCT that utilizes a local  $x'-y'$  system (see Fig. C1) is used [Johnson (1987); Smith and Raju (1998)]. The location of the nodes  $j$  and  $i$  shown in Fig. C1(b) are used to determine a local  $x'$  axis of the rotated coordinate system. The expressions for  $G_I$  and  $G_{II}$  in the local coordinate system can be written using the notation shown in Fig. C1 as:

$$G_I = -\frac{1}{2\Delta c} \left[ Y'_i(v'_m - v'_{m^*}) + Y'_j(v'_l - v'_{l^*}) \right] \quad (C3)$$

$$G_{II} = -\frac{1}{2\Delta c} \left[ X'_i(u'_m - u'_{m^*}) + X'_j(u'_l - u'_{l^*}) \right] \quad (C4)$$

where

$\Delta c$  is the crack growth increment, and is equal to the size of the elements at the crack tip,

$X'_i, Y'_i$  are the nodal forces at node  $i$  evaluated using the elements I and J in the  $x'$  and  $y'$  directions respectively,

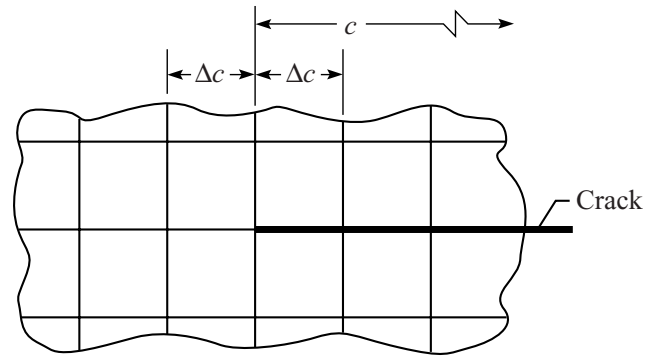
$X'_j, Y'_j$  are the nodal forces at node  $j$  evaluated using the element I in the  $x'$  and  $y'$  directions respectively,

$u'_m, u'_{m^*}, u'_l, u'_{l^*}$  are displacements in the  $x'$  direction at nodes  $m, m^*, l$ , and  $l^*$  respectively, and

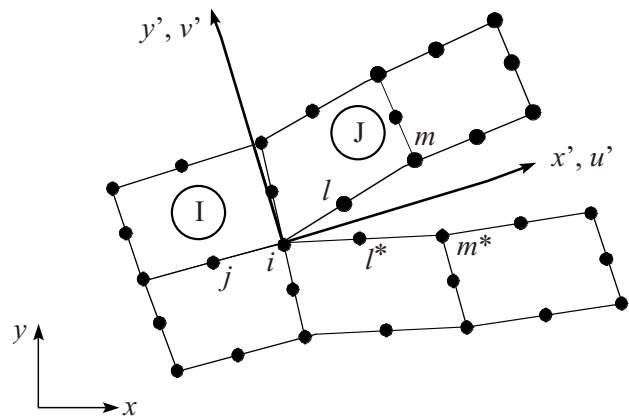
$v'_m, v'_{m^*}, v'_l, v'_{l^*}$  are displacements in the  $y'$  direction at nodes  $m, m^*, l$ , and  $l^*$  respectively.

The values of the forces and displacements on the right hand sides of equations (C3) and (C4) are extracted from a FE analysis.

For a linear analysis, the forces and displacements  $X', Y', u',$  and  $v'$  on the right sides of equations (C3) and (C4) are



a) Undeformed shape.



b) Deformed shape.

**Figure C1:** Model and notation used in virtual crack closure technique.

linear with respect to the applied load  $F$ . The total strain energy release rate  $G_T$  is calculated from the sum of the products of these quantities and hence is proportional to  $F^2$ .

**Appendix D: Linear vs. Nonlinear Analysis of Bonded Joints and Computational Techniques Used for Calculating Derivatives of  $G_T$**

In Fig. D1, the derivative of  $G_T$  with respect to  $F^2$  (the slope in Fig. 5) is plotted as a function of the applied load  $F$ . Note that for the linear case the derivative is a constant, while for the nonlinear case the derivative is not a constant. The derivatives for the linear case and

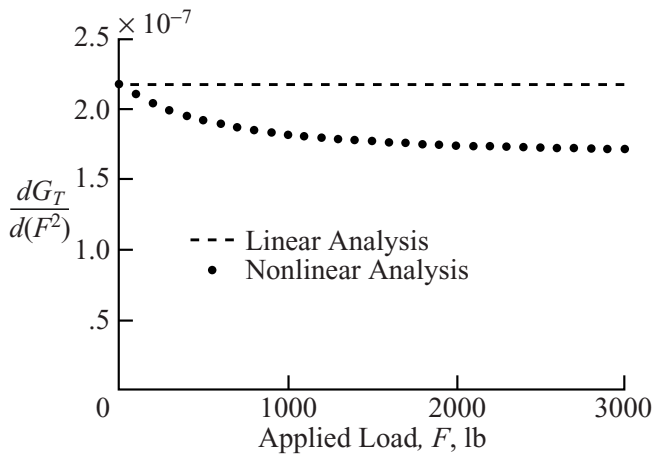


**Figure D1:** Derivative of  $G_T$  with respect to  $F^2$ .

nonlinear case are the same at  $F = 0$ , but the derivatives differ for other values of  $F$ .

Fig. D2 provides a more dramatic contrast between the linear and nonlinear analyses. In this figure, the second derivative of  $G_T$  with respect to  $F^2$  is plotted as a function of the applied load  $F$ . For the linear case, the second derivative is zero for all values of the load  $F$ . For the nonlinear case, the second derivative is relatively large near  $F = 0$ , then drops by three orders of magnitude near  $F = 2000$  lb.

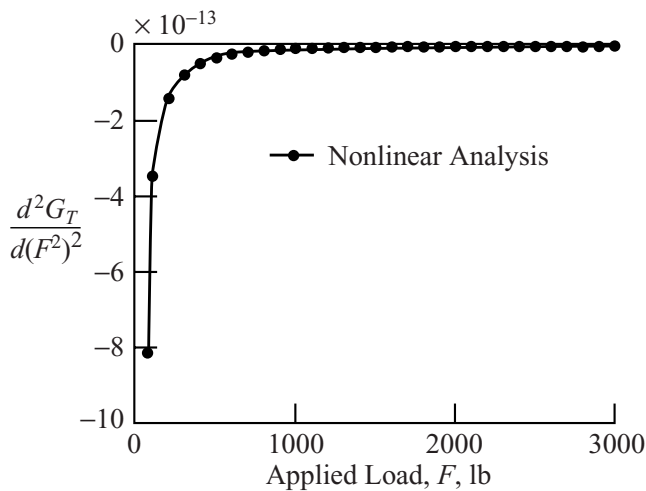


**Figure D2:** Second derivative of  $G_T$  with respect to  $F^2$ .

Based on the results presented in Figs. D1 and D2, the nonlinear analysis curve in Fig. 5 can be interpreted as

follows. At  $F = 0$  the slope of the nonlinear analysis curve is equal to the slope of the line for the linear solution. For values of  $F$  between zero and 2000 lb, the slope of the curve becomes smaller as the joint straightens and stiffens. The nonlinear analysis accounts for that straightening and stiffening. During straightening,  $G_T$  is not linear with respect to  $F^2$ . For values of  $F$  greater than about 3000 lb,  $G_T$  is nearly linear in  $F^2$  with a slope that is smaller than that calculated from the linear analysis. In summary, the geometrically nonlinear analysis accounts for the joint rotation, straightening, and stiffening, while the linear analysis does not account for these phenomena. Because of the scale, the progress of the rotation, straightening, and stiffening cannot be seen in Fig. 5, but the changes can be seen clearly in Figs. D1 and D2.

The data in Figs. D1 and D2 were obtained using a combination of chain rule differentiation and finite difference approximations. The chain rule differentiation provided expressions containing derivatives of  $G_T$  with respect to  $F$  rather than  $F^2$ . That change was made because the values of  $G_T$  were calculated at equal increments in  $F$  (100 lb increments) rather than equal increments in  $F^2$ . As a result, multipoint finite difference approximations could be more accurate for derivatives with respect to  $F$  than for derivatives with respect to  $F^2$ .

For example, for Fig. D2, chain rule differentiation provides the following expression

$$\frac{d^2G_T}{d(F^2)^2} = \frac{1}{4F^2} \frac{d^2G_T}{dF^2} - \frac{1}{4F^3} \frac{dG_T}{dF} \tag{D1}$$

The values of the derivatives on the right hand side in equation (D1) were calculated using 4- and 5-point finite difference approximations. The value of  $\frac{d^2G_T}{d(F^2)^2}$  at  $F \approx 70$  lb was calculated with a 2-point central difference formula. The computational technique described above was most valuable in calculating  $\frac{d^2G_T}{d(F^2)^2}$  for small values of  $F$  where that derivative is changing rapidly.